Chapter 4

Calculations with a box diffusion carbon cycle model

4.1 Introduction

This chapter focuses on calculations with a box diffusion carbon cycle model to quantify interpretation of some of the features in the Law Dome ice core CO_2 and $\delta^{13}C$ record. The box diffusion model (BDM) is a standard tool for investigating long term changes in the carbon cycle. The fact that it is a simple model makes it possible to try an extensive range of calculations. The model used here was developed by Enting and Lassey (1993) and is based on the original box diffusion model introduced by Oeschger et al. (1975). A particular feature of this model is that parameters are calibrated using a Bayesian technique. Two enhancements will be added to the Enting-Lassey model (temperature dependence of fluxes and time variations in the natural production of ^{14}C) and the model will be recalibrated, making use of the Law Dome CO_2 record. In addition to CO_2 and $\delta^{13}C$, ^{14}C will be described in this chapter, as ^{14}C plays an important role in model calibration.

The model will first be used in forward mode, where CO_2 and $\delta^{13}C$ are calculated for specified fluxes. This calculation is useful to show how much of the observed variation in CO_2 and $\delta^{13}C$ can be explained by current estimates of a number of sources and sinks. The appropriateness of using time varying natural ^{14}C production will be discussed. This is followed by calculations exploring the response of CO_2 and $\delta^{13}C$ to temperature changes. The model will also be used for a single deconvolution calculation which tracks the Law Dome CO_2 record. A number of aspects of this calculation will be discussed, including

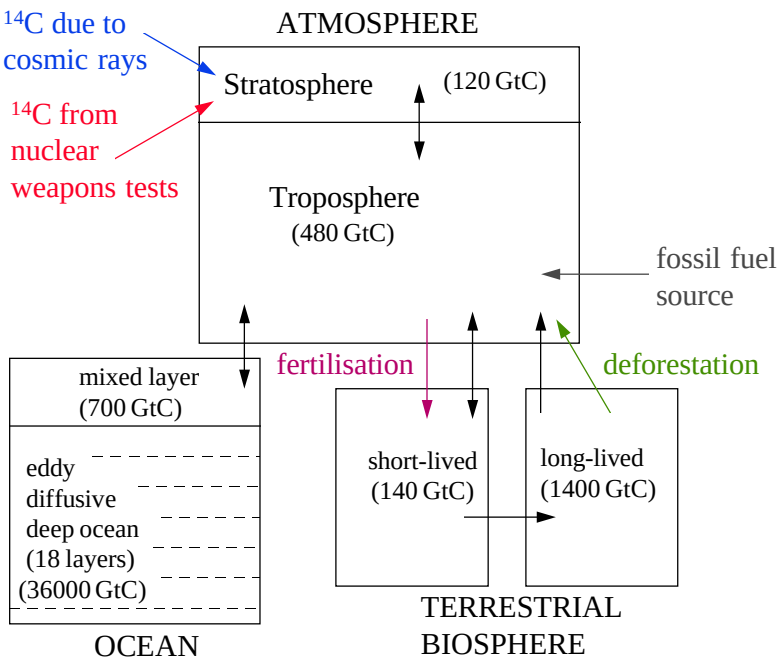

Figure 4.1: Structure of the box diffusion model, showing the fluxes between reservoirs and typical reservoir sizes. The reservoir sizes shown are those that were used by Enting and Lassey (1993).

the overall agreement of δ^{13}C, the bomb ^{14}C budget and the calculated net fluxes. Some of the calculations in this chapter are also described in Trudinger et al. (1999), Francey et al. (1999c) and Francey et al. (2000).

4.2 The box diffusion model

4.2.1 Model description

The box-diffusion carbon cycle model (Enting and Lassey, 1993; Lassey et al., 1996) is a globally aggregated model with 2 well-mixed atmospheric reservoirs (troposphere and stratosphere), a 2-box biosphere (short- and long-lived), a surface ocean layer and an Oeschger et al. (1975) diffusive deep ocean. Figure 4.1 shows the model structure. In addition to CO_2, the isotopes ^{13}C and ^{14}C are modelled.

The calculations described in this chapter include a prescribed source of CO_2 to the atmosphere due to fossil fuel burning. The forward calculations include a flux from the long-lived biosphere to the atmosphere due to land-use change, and enhancement of net

primary production (NPP) due to CO_2 fertilisation, which uses the hyperbolic form given by Allen et al. (1987), (see Enting and Lassey (1993) for details).

The model has two types of detrital flux in the ocean, organic and carbonate, which each have different penetration depths and amounts of isotopic fractionation relative to the inorganic carbon in the surface water (Enting and Lassey, 1993). The rate of remineralisation of the organic component decreases with depth following a power law given by Martin et al. (1987), while the carbonate component dissolves equally at all depths. The pCO_2 of the mixed layer is given by

$$P = P_0[1 + y\xi(y)] \tag{4.1}$$

where P_0 is a reference partial pressure in ppmv (set to the pre-industrial CO_2 concentration in the atmosphere), $y = (q - q_0)/q_0$, q is the dissolved inorganic carbon concentration, with $q_0 = 2.089$ moles m^{-3} and the buffer factor, ξ, is given by

$$\xi(y) = 9.36 + 59.56y + 4558y^3 \tag{4.2}$$

from Bacastow (1981).

One enhancement that is made to the Enting-Lassey model is to include the effect of changes in temperature on exchange between reservoirs, which is modelled as follows. The response of the biospheric fluxes to changing temperature uses the Q_{10} relationship,

$$F(T + \Delta T) = F(T) \times Q_{10}^{\Delta T/10} \tag{4.3}$$

where $F(T)$ is the flux at temperature, T, and $Q_{10} = 2.0$ for respiration and 1.4 for NPP. These are typical Q_{10} values, and were used by Harvey (1989) in a number of globally aggregated terrestrial biosphere models. Defining global Q_{10} values is difficult. For the calculations presented here, what matters more than the actual Q_{10} values is the fact that, globally speaking, respiration is more sensitive to temperature than NPP, which is what is expected (J. Lloyd, pers. comm.). This can be verified for particular ecosystems. For example, Grace et al. (1996) showed that for a tropical rainforest, respiration is far more sensitive to temperature than is photosynthesis. In general, photosynthesis is less sensitive to temperature than respiration, especially at lower CO_2 concentrations. As NPP is the balance between plant respiration and photosynthesis, the Q_{10} value for NPP lies between the values of Q_{10} for plant respiration and photosynthesis, so is less than

the respiration value. The sense of the change in CO_2 and the isotopes should be fairly reliable, however the magnitude of the change will be difficult to determine correctly with a globally aggregated biospheric model such as the one used here.

For the ocean, the temperature-dependence of the buffer factor, ξ, is modelled as in Enting and Pearman (1982), with the ocean partial pressure of CO_2 varying with temperature according to

$$P(T) \propto \frac{1 + 0.0389T + 0.000448T^2}{1780 - 20T} \tag{4.4}$$

where T is in °C. This comes from considering the temperature dependence of the reaction equilibrium constant, K, and solubility, α, in equation (2.5). Temperature dependence of K is determined using data from Broecker and Peng (1974) as

$$K = 1780 - 20T \tag{4.5}$$

and α has temperature-dependence

$$\frac{\alpha_0}{\alpha} \simeq 1 + 0.0389T + 0.000448T^2 \tag{4.6}$$

determined using tabulated data from Hodgeman (1958), where α_0 is the solubility at 0°C.

Temperature-dependence of isotopic fractionation of air-sea exchange follows Heimann and Keeling (1989) in using

$$\alpha_{ma} = \alpha_{am}\left(1.02389 - \frac{9.483}{T + 273.15}\right) \tag{4.7}$$

which equates the temperature-dependence of the kinetic fractionation factor for sea-air flux, α_{ma}, with the equilibrium fractionation of gaseous CO_2 with respect to dissolved HCO_3^- measured by Mook et al. (1974), and assumes α_{am} (kinetic fractionation factor for air-sea flux) is constant. This gives very similar results to the temperature-dependence given by Zhang et al. (1995) for total DIC. The model uses temperature anomalies as deviations from 17°C for the ocean fluxes. This value was suggested by T. Hirst (CSIRO, pers. comm., 1995) as a reasonable estimate of the pre-industrial global average sea-surface temperature. (Variations in isotopic fractionation of biospheric exchange are assumed to be negligible.)

^{14}C from bomb detonation and natural production due to cosmic rays are both put into the model stratosphere. The other enhancement to the model is to include time variation

in the natural production rate of ^{14}C. This is done using a record of ^{10}Be (see Section 2.6), with

$$^{14}\text{C prod} = A + B\left(^{10}\text{Be}(t) - C\right) \tag{4.8}$$

where A is the mean global ^{14}C production rate, C is a mean ^{10}Be concentration and B scales variations in ^{10}Be concentration to ^{14}C production. A, B and C are all tuned in the model's overall calibration procedure. The mean ^{10}Be concentration, C, is tuned rather than just using the mean for the particular record. The record mean may not be the same as the long-term mean, around which variations are assumed to be proportional to variations in global ^{14}C production rate.

The model parameters are calibrated using a Bayesian calibration technique, which is described by Enting and Lassey (1993), and also by Enting and Pearman (1987) for a slightly different model configuration. Briefly, the calibration procedure tunes the model parameters to minimise the sum of squares of differences between model results and observations, as well as the sum of squares of deviations of the parameters from independent prior estimates of the parameters. The prior estimates of the parameters are included to stabilise the calibration, and to make use of the fact that the range of reasonable values is already known for most of the parameters. An important advantage of the model's calibration technique is that many of the model parameters can be tuned simultaneously, and to a number of very different types of data, rather than having to tune the different components of the model separately.

4.2.2 Model parameters and input data

Data used to calibrate the model are the following: 75 tree-ring Δ^{14}C measurements between 1200–1945 from Stuiver and Becker (1993), needed primarily to tune the parameters that use ^{10}Be to reconstruct ^{14}C production rate variations (the Δ^{14}C tree-ring data are detrended, as will be explained in Section 4.3.1); 2 ocean-surface Δ^{14}C values, (-59 ‰ in 1958 and 110 ‰ in 1973) based on Broecker et al. (1960) and GEOSECS (Broecker et al., 1985a); 2 bomb ^{14}C ocean inventories (difference of 1974 and 1975 from 1955 giving 299 and 311 $\times 10^{26}$ atoms, respectively) from Duffy and Caldeira (1995), based on GEOSECS, but adjusted to be global values using a 3-D ocean model; 6 tropospheric Δ^{14}C values, 1967–1987; 4 stratospheric ^{14}C inventories from Tans (1981), which are based on measure-

ments by Telegadas (1971); 1 Δ^{14}C deep ocean value (-150 ‰ in 1973) from GEOSECS; 1 deep ocean ΣCO_2 (2.34 in 1973) from GEOSECS; 7 atmospheric CO_2 values from the Law Dome record between 1794 and 1990, chosen to roughly define the industrial increase (only used in forward calculation). δ^{13}C data are not used for calibration, but the model calculates δ^{13}C, which is compared with the Law Dome δ^{13}C ice core record. ^{13}C therefore acts as an important independent check on the model.

The model calculations start with an initial state in equilibrium. The possible problems associated with making this steady state assumption are minimised by beginning the calculations at a flat part of the ice core record. The earliest relatively steady period in the Law Dome CO_2 record is around 1200, and the calculations are started then, assuming that, at that time, the carbon cycle was close to equilibrium.

Estimates of the source due to fossil fuel burning used in this chapter are from Keeling (1997) between 1860 to 1949, with a linear increase from zero between 1840 to 1860, and from Marland and Boden (1997) after 1950. These values are very similar to the more recent estimates by Marland et al. (1999) shown in Figure 2.11a. The δ^{13}C of the fossil-fuel source is taken from Andres et al. (2000) (Figure 2.11b). Land-use change estimates are from Houghton (1995a). These land-use change estimates are net fluxes. If they were used directly in the model, the size of the long-lived biosphere would gradually decrease. This would cause a decrease in the model-calculated respiration flux from the biosphere, because (in the model) the long-lived biosphere box has a fixed turnover time. The net effect would then be different from the Houghton (1995a) net flux estimates. In other words, the net biotic flux, $B(t)$, in the model is a sum of forcing, $D(t)$, and a relaxation to equilibrium. Houghton's estimates of $B(t)$ need to be converted to $D(t)$ by using

$$D(t) = B(t) + \lambda_L \int_{1700}^{t} B(t')dt' \tag{4.9}$$

where λ_L is the inverse turnover time of the long-lived biosphere. The quantity $D(t)$ has no real significance in terms of land-use change fluxes, but is a model-dependent quantity needed to ensure that the net flux matches the given estimates. It is required because the long-lived biospheric reservoir includes both undisturbed and disturbed systems so its size is not fixed. This is described further in Enting and Lassey (1993).

The bomb detonation history of Enting (1982) is used, and the amount of ^{14}C per megaton TNT equivalent yield is tuned in the model's calibration procedure. The ^{10}Be

ice core record from South Pole (Raisbeck et al., 1990) is used for calculating the natural production of ^{14}C due to cosmic rays. It turns out that the tuned mean ^{10}Be, (i.e. variable C in equation (4.8)) is very close to the mean for the record.

The model is calibrated separately for the forward and single deconvolution calculations. Table 4.1 lists the model parameters for both cases. Prior estimates and uncertainties are given for those parameters which were tuned in the present calibration procedure. The biospheric reservoir sizes and fluxes are not calibrated, but have been chosen to give the same isotopic pulse response as the biospheric model of Emanuel et al. (1981). Other parameters and many of the prior estimates use values from Enting and Lassey (1993), which were used in the IPCC calculations (Enting et al., 1994). The atmospheric turnover time and ocean diffusivity values are typical of other estimates. The stratospheric turnover time is short compared to other estimates of around 3 years (this will be discussed briefly in Section 4.4.2), and the detrital fluxes are perhaps on the low end of current estimates.

4.3 Forward calculations

Figures 4.2a–h show calculated CO_2, $\delta^{13}C$ and ^{14}C for the forward model run compared to a number of different observations, only some of which have been used to calibrate the model. In general, the filled symbols indicate data used for calibration. The tuned model parameters for this run are listed in column 3 of Table 4.1. The net fluxes are shown in Figure 4.2d, where the biospheric flux is the sum of land use change and uptake due to fertilisation. The model gives quite good agreement with all of the observations. Tropospheric and stratospheric ^{14}C drops too slowly after the bomb pulse – the bomb budget will be discussed in more detail in Section 4.4.2. The initial CO_2 level is fixed and the 1990 CO_2 observation has a small uncertainty, so the CO_2 change acts as a strong constraint on the model parameters. The modelled CO_2 change agrees well with the other CO_2 observations. The initial $\delta^{13}C$ level is tuned. A tightly constrained $\delta^{13}C$ observation in 1990 anchors the modelled $\delta^{13}C$, but as no other $\delta^{13}C$ observations are used, the change in $\delta^{13}C$ does not at all influence calibration of the model parameters. The fact that the modelled $\delta^{13}C$ change from pre-industrial levels to the present is very close to observed is a very important result. Figure 4.3 shows CO_2 and $\delta^{13}C$ variations from the forward calculation for 1800-1990 compared with the Law Dome record. Although

Parameter	Fixed	Fwd	Single	Prior	Uncert
ocean surface layer depth (m)	75				
ocean depth (m)	3800				
ocean surface area (10^{12} m)	361.16				
tropospheric : stratospheric mass ratio	80:20				
ppm per Gt in the atmosphere	0.47				
deep ocean diffusivity (m^2 y^{-1})		5292	5524	5364	2000
atmospheric C turnover w.r.t. ocean (y)		9.16	8.76	12	2
stratospheric C turnover time (y)		2.0	1.8	4.0	1.0
net primary productivity (GtC y^{-1})	84.3				
turnover time of young biosphere to atmosphere (y)	6.3				
turnover time of young biosphere to old biosphere (y)	20.3				
turnover time of old biosphere (y)	54.5				
size of young biosphere (Gt)	405.3				
size of old biosphere (Gt)	1089				
fraction of NPP fertilised by excess CO_2		0.81	–	0.7	0.3
bomb ^{14}C production (10^{26} atoms per Mt TNT yield)		3.15	3.07	2.75	3.0
A = mean ^{14}C production due to cosmic rays (10^{26} atoms y^{-1})		2.54	2.56	2.5	1.5
B = factor relating ^{10}Be variations to ^{14}C production variations ($10^{-3} \times (10^{26}$ atom ^{14}C $y^{-1})$ / (10^2 atoms g^{-1}))		5.070	5.085	4.0	12.0
C = mean ^{10}Be concentration (10^2 atoms g^{-1})		384	384	382	7
detrital parameters					
carbonate flux (Gt y^{-1})		2.20	2.37	4.0	3.0
organic flux (Gt y^{-1})		3.41	3.28	4.0	3.0
carbonate isotopic fractionation (‰)	0				
organic isotopic fractionation (‰)	-24				
isotope fractionation factors ($^{13}C/^{12}C$)					
atmosphere - ocean	0.99795				
ocean - atmosphere	0.9892				
atmosphere - biosphere	0.982				
biosphere - atmosphere	1				

Table 4.1: Model parameters for the BDM. 'Fixed' parameters are specified, 'Fwd' and 'Single' parameters are calibrated by the model in forward and single deconvolution calculations, respectively. Prior estimates and (prior) uncertainties are given for the tuned parameters.

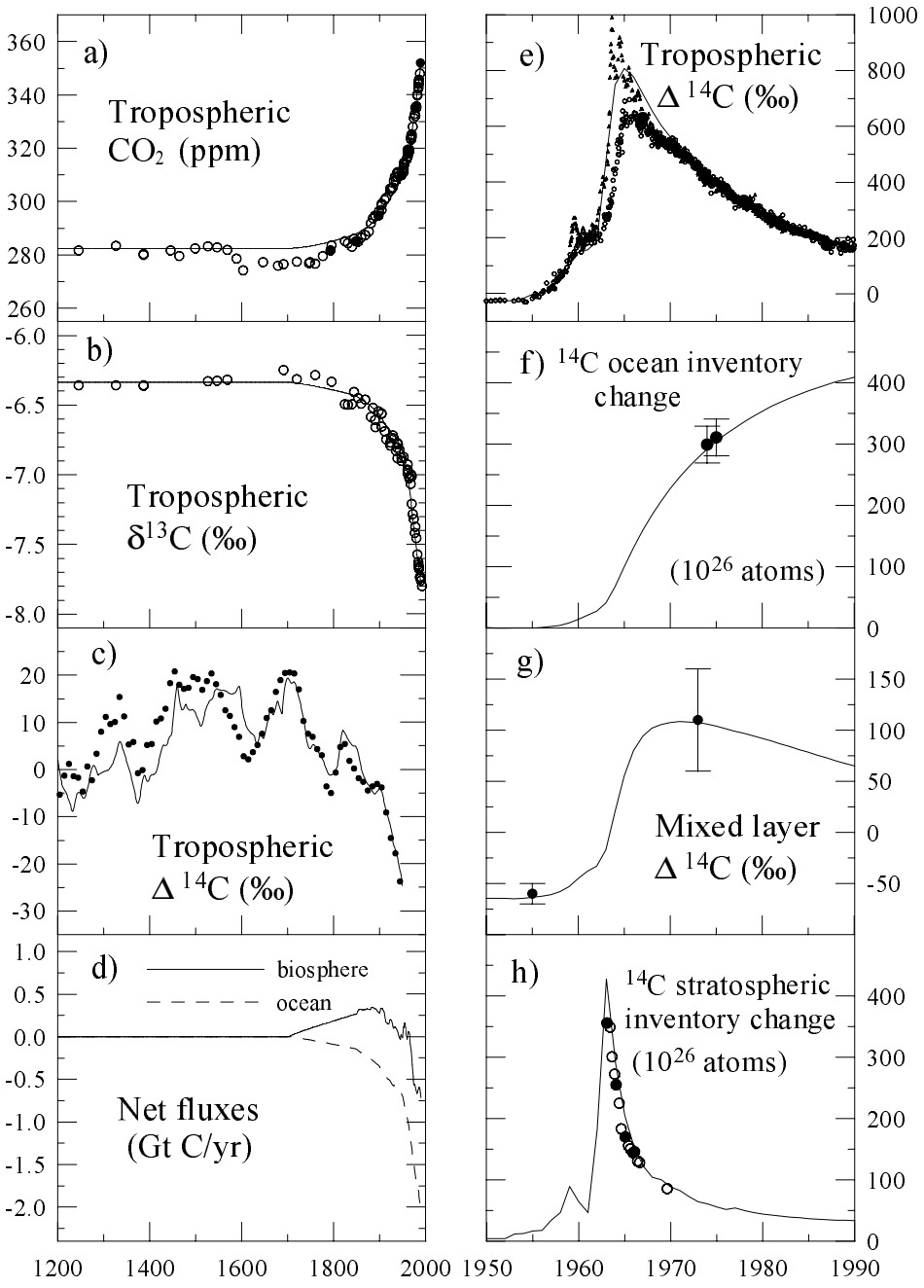

Figure 4.2: Forward calculation with box diffusion model. (a) Law Dome CO_2 record and modelled CO_2 (b) Law Dome $\delta^{13}C$ record and modelled $\delta^{13}C$. (c) Calculated young biospheric $\Delta^{14}C$, with observations from Stuiver and Becker (1993). (d) Net biospheric (solid line) and oceanic (dashed line) flux used in the forward calculation. (e) Tropospheric $\Delta^{14}C$. Observations are from New Zealand, (Manning and Melhuish,1994) (circles) and Vermunt, Austria (Levin et al. 1985) (triangles). (f) Bomb ^{14}C ocean inventory, with data from Duffy and Caldeira (1995). (g) Mixed layer $\Delta^{14}C$. (h) Stratospheric ^{14}C inventory, with data from Tans (1981).

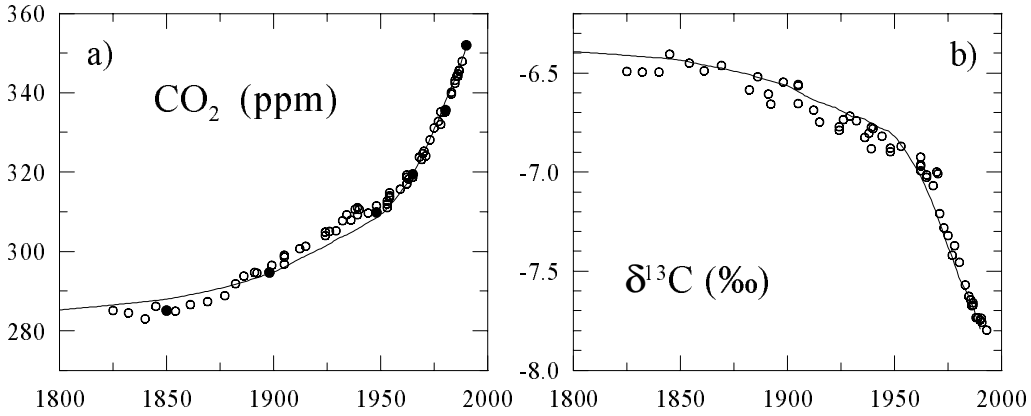

Figure 4.3: a) CO_2 and b) $\delta^{13}C$ from the forward model calculation and the Law Dome record. The solid symbols in a) show 6 of the 7 CO_2 data used for calibration.

the overall modelled change in CO_2 and $\delta^{13}C$ over the industrial period agrees well with observations, many of the observed multi-decadal to century time scale variations are not captured with this calculation. The results show the change due only to fossil fuel burning, Houghton's estimates of land use change, ocean uptake and CO_2 fertilisation. The effect of climate variations, which is a major forcing mechanism for both biospheric and oceanic exchange, is not included. In addition there may be fluxes due to land use change (e.g. the PIAGREV) that are not included in the Houghton estimates, as discussed in Section 2.9.1.

Modelled CO_2 is lower than the ice core record between about 1910 and 1950. The model rejoins the ice core record after the observed period of low growth rate in the 1940s. (There were no CO_2 data used for calibration through this period, but even if there had been the results would probably have been very similar, as the decadal scale variation is quite limited in the forward calculation.) Compared with the specified inputs, there appears to have been extra release of CO_2 up to almost 1940, then extra uptake through the 1940s. The deconvolution calculations will be able to quantify the fluxes required to match the CO_2 record.

4.3.1 ^{14}C production from ^{10}Be data

Figure 4.2c shows tree-ring $\Delta^{14}C$ measurements from Stuiver and Becker (1993) with modelled $\Delta^{14}C$ from the forward calculation. The South Pole ^{10}Be record from Raisbeck et al. (1990) was used to determine variations in ^{14}C production rate. The parameters A,

B and C in equation (4.8) were tuned in the model's calibration procedure. Variations in the production rates of both ^{10}Be and ^{14}C are related to changes in cosmic ray flux, and are therefore very similar, but the geochemical behaviour of the two isotopes in the atmosphere is quite different. ^{14}C is oxidised to $^{14}CO_2$, which is quite well mixed in the atmosphere, and becomes involved in exchange between reservoirs. ^{10}Be attaches to aerosols, and is removed from the atmosphere after a mean residence time of no longer than 1 to 2 years (Beer et al., 1994). This means that ^{10}Be can have significant spatial variability. According to Bard et al. (1997), ^{10}Be measured in Antarctic ice is mainly produced at high latitudes. Solar modulation is higher at high latitudes than at the equator due to the orientation of the magnetic field, so the relative amplitude of ^{10}Be variations around the mean in polar ice cores probably over-estimates variation in global production. Bard et al. used a 'Polar Enhancement Coefficient' (PEC) of about 0.6 to take account of this effect. The parameter B in equation (4.8) includes this effect in its conversion from ^{10}Be concentration to global ^{14}C production rate. The tree-ring data in Figure 4.2c are detrended for the long-term increase due to the change in the earth's geomagnetic field intensity by subtracting the sinusoidal function derived by Houtermans (1971) and given in Stuiver and Quay (1980). South Pole ^{10}Be reflects mainly polar production, which should not be affected much by variations in the geomagnetic field. Bard et al. (1997) also detrended the ^{14}C data for comparison with model results.

The main reason for reconstructing ^{14}C production rate variations from ^{10}Be was so that the ^{14}C Suess effect could be used as a stronger constraint for calibrating the model parameters. Figure 4.4a shows the calculated Δ^{14}C for constant and varying natural production rates (dotted line). The model parameters have been recalibrated for the constant production case, with only small differences between parameter values for the two cases. The calculations already described used the South Pole ^{10}Be record (Raisbeck et al., 1990). Figure 4.4b shows the calculated Δ^{14}C for a different ^{10}Be record, that from Dye 3, Greenland (Beer et al., 1994). Again the model has been recalibrated, with small differences in the parameters.

The use of the ^{10}Be-derived ^{14}C production rate compared to a constant production rate does give a much better fit to the observed Δ^{14}C, although there are differences in the time variations due to the two ^{10}Be records. In particular, the Suess effect is certainly

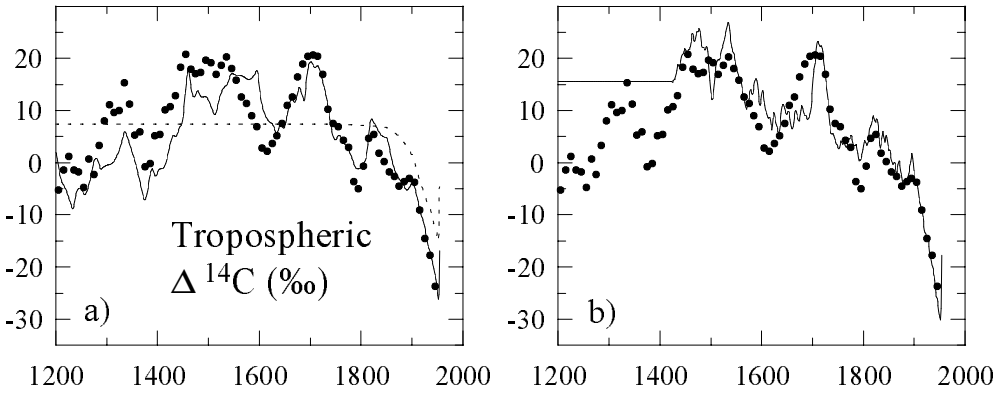

Figure 4.4: a) $\Delta^{14}C$ calculated with South Pole ^{10}Be variations (solid line) and constant production rate (dotted line). b) $\Delta^{14}C$ calculated with Dye 3 ^{10}Be record (Beer et al., 1994).

better captured with the varying production rate. Current uncertainties in the use of a single record of ^{10}Be to reconstruct ^{14}C production rates (i.e. spatial variability of ^{10}Be and the need for a PEC) mean that fitting the Suess trend doesn't presently help constrain model parameters such as the turnover times of the reservoirs. A composite record with ^{10}Be from different sites, perhaps combined with other measures of cosmic ray variations would give better estimates of the ^{14}C production rate, so that pre-bomb ^{14}C could be used more confidently for carbon cycle model calibration.

As an aside, it is interesting to look at the inventories of ^{14}C over recent centuries, and note the effect of the input of CO_2 due to fossil fuel burning and deforestation. A result that is, at first, a little surprising is that the amount of ^{14}C in the atmosphere actually *increases* due to the addition of (^{14}C free) fossil fuel CO_2. $\Delta^{14}C$, as expected, decreases. Figure 4.5a, 4.5b and 4.5c show modelled ^{14}C inventories, calculated with a constant ^{14}C production rate, for fossil fuel and deforestation sources modelled separately and together in the forward model calculation. The unexpected increase in atmospheric ^{14}C due to fossil fuel burning (Figure 4.5a) occurs because the increase in mixed layer DIC affects the chemical equilibrium between DIC and CO_2 gas in the mixed layer. (Equation (4.2) shows how the buffer factor depends on DIC in the model.) The equilibrium for ^{14}C is also changed, and this results in more ^{14}C in the dissolved CO_2 gas state and less in the carbonate state and therefore a flux of ^{14}C to the atmosphere. Deforestation causes a

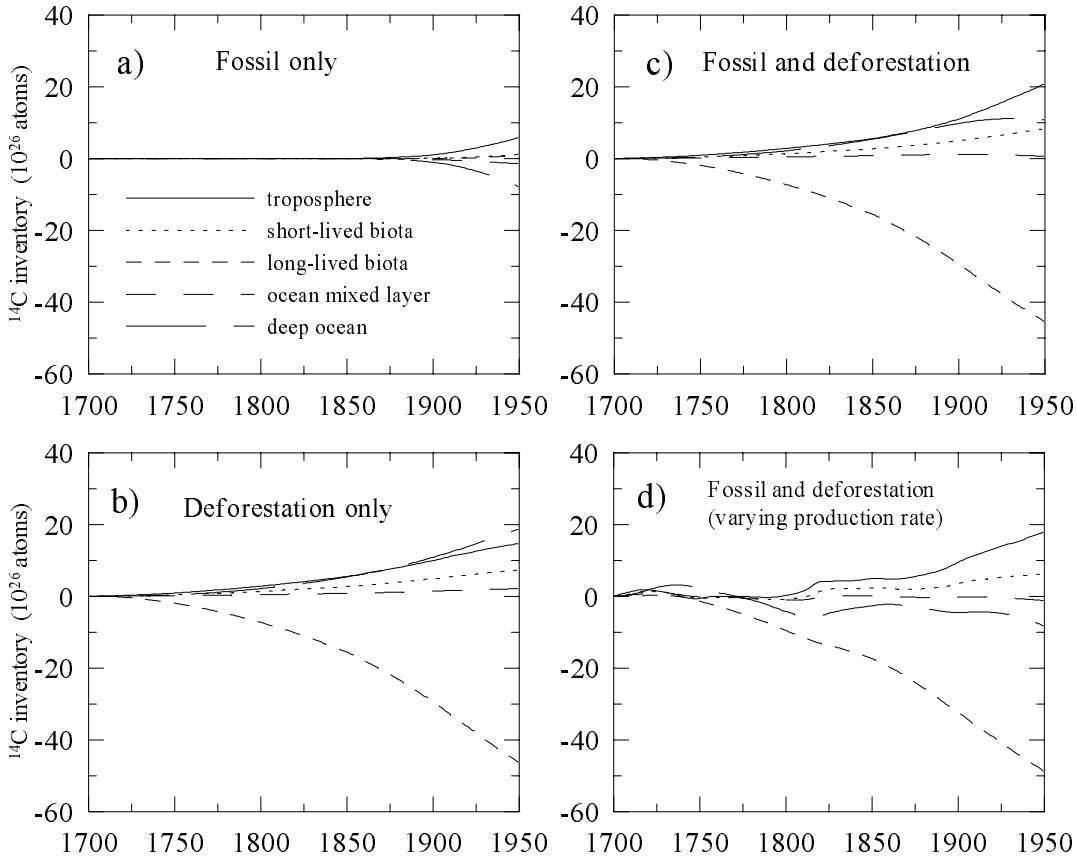

Figure 4.5: Calculated ^{14}C inventories (10^{26} atoms) for a) fossil fuel source, b) deforestation source and c) fossil and deforestation with constant natural production rate. d) Inventories for fossil fuel and deforestation with a varying natural production rate (South Pole ^{10}Be, calculation begins in 1700).

decline in total carbon and ^{14}C in the long-lived biota. The ^{14}C from the long-lived biota is transferred to the other reservoirs (Figure 4.5b). Figure 4.5c shows the inventories for both fossil fuel burning and deforestation, and Figure 4.5d shows the results modelled with a varying natural production rate. These model results were presented by R. J. Francey at the Seventh International Conference on Accelerator Mass Spectrometry, in Tucson, USA in May 1996, and are described in Francey et al. (2000). Since then Caldeira et al. (1998) have also modelled this effect. They predicted that sometime in the next few years the ^{14}C flux from the ocean to the atmosphere due to the input of fossil fuel CO_2 will balance and then overwhelm the uptake of bomb ^{14}C by the ocean.

4.3.2 Little Ice Age calculations

A particularly striking feature in the Law Dome CO_2 record is the low CO_2 level between about 1550 and 1800, coinciding with the period often referred to as the 'Little Ice Age' (see Section 2.9.2). As discussed by Etheridge et al. (1996), the decrease in CO_2 is unlikely to have been the primary cause of the LIA cooling. It is more likely that the reduced temperature (driven by other factors) affected the carbon exchange between different reservoirs, changing the global CO_2 concentration level. $\delta^{13}C$ over this period is higher than the mean pre-industrial level, and this fact is explored as a means of determining the most likely processes involved.

In particular, the possible role of temperature in causing these changes in CO_2 and $\delta^{13}C$ is investigated, by modelling separately the response of oceanic and terrestrial exchange to a decrease in temperature. A hypothetical temperature record is used, where temperature decreases linearly between 1550–1600 then stays constant until 1750, when it increases linearly to its initial level in 1800 (Figure 4.6a). The magnitude and timing of the temperature change are very idealised, and were chosen so that modelled CO_2 would roughly match the changes in the CO_2 ice core record. It should be kept in mind, as discussed in Section 2.9.2, that although the term 'Little Ice Age' is quite widely used, there is no consensus on when the LIA began or ended, and there is no evidence in temperature records of a worldwide, synchronous and prolonged cold interval (Jones and Bradley, 1992b). Grove (1988) estimated that the observed temperature decrease in parts of Europe was about 1–2°C, with frequent fluctuations rather than sustained low temperatures. A cooling of 1°C for the whole biospheric or oceanic reservoirs will be considered, but the modelled changes would also apply for a temperature change of more than 1°C over a smaller region.

The carbon cycle model is used in forward mode to calculate the change in CO_2 and $\delta^{13}C$ with the hypothetical temperature perturbation affecting either biospheric or oceanic exchange. The solid line in Figure 4.6b shows modelled CO_2 due only to fossil fuel burning, land-use change and CO_2 fertilisation (plus ocean uptake as calculated by the BDM). As well as these sources and sinks, temperature-dependent terrestrial exchange (long dashes) and temperature-dependent oceanic exchange (short dashes) is included. In both cases, the decrease in temperature causes a decrease in global CO_2. Figure 4.6c shows the calculated

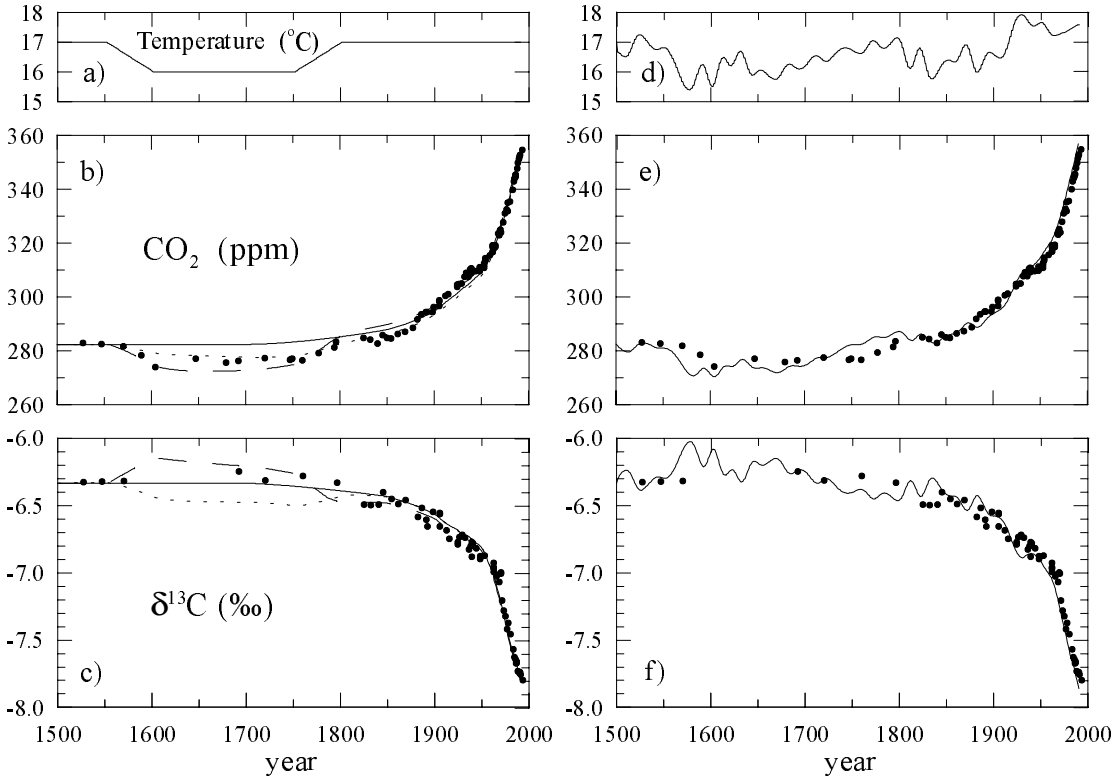

Figure 4.6: Forward calculations with box diffusion model. (a) Hypothetical temperature record used in the LIA model calculations, (b) Modelled CO_2 and (c) modelled $\delta^{13}C$. All three cases shown in (b) and (c) include the fossil fuel burning, land-use change and CO_2 fertilisation. In addition we include temperature-dependent terrestrial exchange (long dashes) and oceanic exchange (short dashes) for the hypothetical temperature record. (d) Northern hemisphere summer temperature anomaly from Bradley and Jones (1993). (e) CO_2 and (f) $\delta^{13}C$ calculated using a forward run with fossil fuel, land-use change, CO_2 fertilisation and temperature-dependence of biospheric exchange with the Bradley and Jones (1993) temperature record.

$\delta^{13}C$ for the same 3 cases. The effect of the temperature decrease on isotopic fractionation causes a decrease in $\delta^{13}C$. The temperature response of terrestrial exchange is a reduction in both NPP and soil respiration, with the reduction in soil respiration dominating. This leads to an increase in $\delta^{13}C$, which is what is measured in the ice core record.

If the temperature change had affected both terrestrial and oceanic exchange, the model would give addition of the CO_2 decrease and partial cancellation of the $\delta^{13}C$ change. However, a scenario consistent with the changes measured in the ice core record is that global sea surface temperatures were not significantly different during the LIA, but that

major terrestrial biomes experienced significant cooling. Many of the proxy temperature records that show the cooling during this period are from northern hemisphere land sites. Information for the southern hemisphere is more limited, with some records suggesting cooling, others showing no cooling. CH_4 from the Law Dome ice cores also shows a decrease through this period, as does the inter-polar difference of CH_4 (Etheridge et al., 1998). Harriss et al. (1993) have argued that lower land temperatures reduce the extent and magnitude of the CH_4 emission flux from northern hemisphere wetlands, the dominant source of pre-industrial CH_4 emissions (Chappellaz et al., 1993). Etheridge et al. (1998) therefore conclude that the lower levels of CH_4 during the LIA were linked to cooling of the northern hemisphere land surfaces, which would be supported by the BDM calculations.

4.3.3 Summer temperature anomaly record

Figure 4.6d shows the northern hemisphere summer temperature anomalies from Bradley and Jones (1993). The CO_2 and $\delta^{13}C$ calculated by modelling the response of the terrestrial biosphere to these temperature variations (as well as fossil fuel burning, land-use change and fertilisation) is shown in Figure 4.6e and 4.6f. The modelled CO_2 and $\delta^{13}C$ shows some features similar to those in the ice core record, however using only a single proxy temperature record does leave many of the features unexplained. It is likely that some regions and biomes have a stronger response to temperature changes than others, and are therefore responsible for more of the variation in global CO_2 and $\delta^{13}C$. In addition, a number of other factors are likely to have just as much effect on global CO_2 and $\delta^{13}C$, e.g. variation in precipitation for biospheric exchange, temperature variation for oceanic fluxes or changes in ocean circulation.

This calculation gives some indication of the different responses of CO_2 and $\delta^{13}C$ to biospheric fluxes. As discussed in Section 2.5, $\delta^{13}C$ responds more than CO_2 to short time scale variations, and an isotopic perturbation disappears more quickly than a CO_2 perturbation. $\delta^{13}C$ in Figure 4.6f shows larger variations due to the temperature changes (relative to the industrial $\delta^{13}C$ perturbation) than does the CO_2 in Figure 4.6e. This is more clearly seen in Figure 4.7, where the CO_2 and $\delta^{13}C$ from the 'no temperature' case (solid lines in Figure 4.6b and 4.6c) is subtracted from the model output for the Bradley and Jones temperature case, then the deviations in both CO_2 and $\delta^{13}C$ are scaled by their respective industrial changes. The $\delta^{13}C$ variations are larger than the CO_2 variations, but

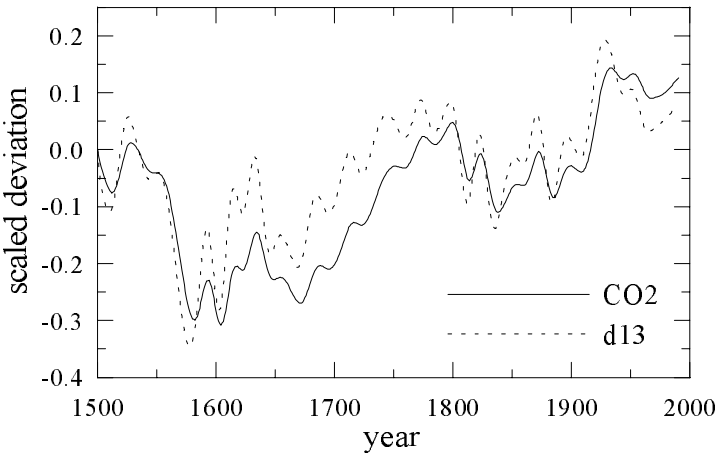

Figure 4.7: Deviations in CO_2 and $\delta^{13}C$ from the model with temperature dependence of biospheric exchange and the Bradley and Jones (1993) temperature record, minus the variations in CO_2 and $\delta^{13}C$, respectively, for the 'no temperature' calculation, then scaled by the respective industrial changes.

don't last as long. Scaling the variations by the industrial perturbation in CO_2 and $\delta^{13}C$ allows useful comparison of CO_2 and $\delta^{13}C$, which have quite different units. The different response functions of CO_2 and $\delta^{13}C$ will be discussed in more detail in Chapter 5.

4.4 Single deconvolution calculation

Forward calculations over long timescales, as described in the previous section, are somewhat limited, as there is not a great deal of source information available. In general, global concentrations are better known than global fluxes. A type of calculation that takes advantage of this fact is the single deconvolution, which tracks CO_2 variations to estimate the biospheric flux (Section 2.10). In the calculations described in this section, the flux due to fossil fuel burning is specified, ocean uptake is calculated by the model and net terrestrial exchange is determined so that the modelled CO_2 follows a spline fit through the Law Dome CO_2 record. The CO_2 spline fit (Figure 4.8a) is a weighted spline, where different ice core measurements are given different weights and this varies smoothing throughout the record. Before 1832, when there is only DSS data, the smoothing varies with data

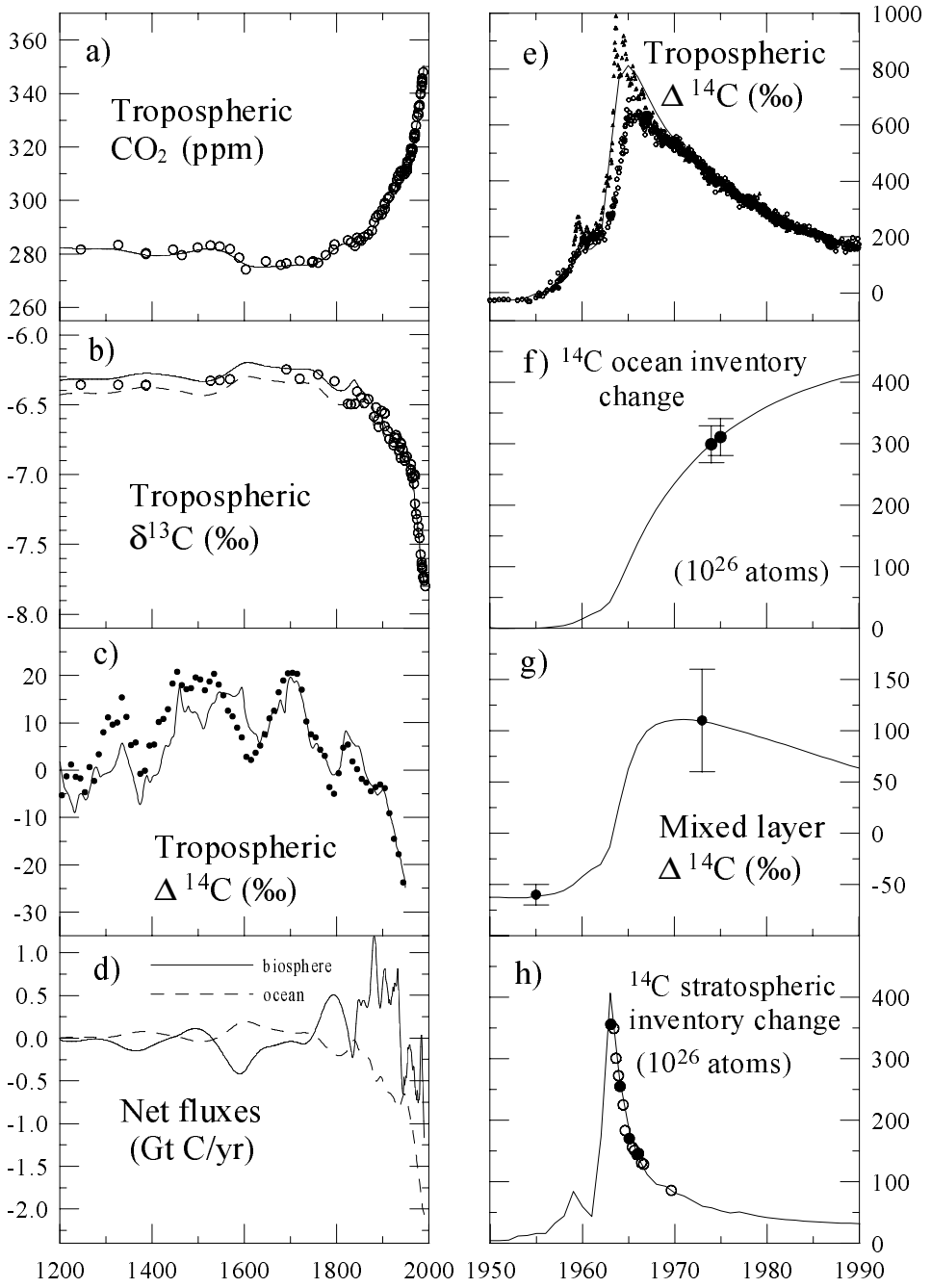

Figure 4.8: Single deconvolution with the box diffusion model. (a) Spline fit to the CO_2 record. (b) Law Dome $\delta^{13}C$ record and modelled $\delta^{13}C$ from the single deconvolution calculation, with CO_2 tracking the spline fit (solid line). The dashed line shows $\delta^{13}C$ calculated with the ocean response to the temperature increase this century. (c) – (h) are as in Figure 4.2 but with the single deconvolution results.

density. After 1832, DE08 and DE08-2 are weighted higher than DSS to take into account the higher time resolution of DE08. The spline has 50% attenuation for periods of about 20 years for the DE08 and DE08-2 measurements, while the smoothing varies for DSS.

The model has been recalibrated for the single deconvolution using the data described in Section 4.2.2 (except that the CO_2 data is not used). Figures 4.8b – 4.8h show model output compared to a number of different observations, only some of which have been used to calibrate the model. Again, the filled symbols indicate data used for calibration.

The calculated $\delta^{13}C$ is shown by the solid line in Figure 4.8b. The initial $\delta^{13}C$ level (in this case, the value at 1200 AD) has been adjusted to ensure that the 1990 $\delta^{13}C$ matches observations. (The initial $\delta^{13}C$ could just as well have been set to the level shown by the ice core record, however as the time rate of change is large in recent years it is difficult to visually distinguish differences in the final $\delta^{13}C$ level.) The modelled 1200-to-modern difference agrees with the Law Dome observations to within the uncertainty of 0.05 ‰ estimated for this quantity by Francey et al. (1999a).

This calculation did not include any effect of variation in temperature. The dashed line in Figure 4.8b shows the $\delta^{13}C$ calculated by including the effect on ocean exchange of the increase in temperature of about 0.5°C that has been measured over this century. For this calculation, the record of observed global temperature from Jones and Briffa (1992) (an earlier version of the data shown in Figure 2.14) was used. The biospheric response to this temperature variation did not need to be modelled, because the biospheric flux is calculated to match the CO_2 spline in either case. The modelled $\delta^{13}C$ pre-industrial – modern difference is reduced by about 0.1 ‰ compared to the constant temperature case, but is still very close to the Law Dome observations. (This case is not shown in any of the other parts of Figure 4.8.)

4.4.1 Calculated net fluxes

The solid and dashed lines in Figure 4.8d show the net biospheric and oceanic fluxes, respectively. These are similar to fluxes calculated by Bruno and Joos (1997) and Craig et al. (1997) who also performed a single deconvolution with the Law Dome CO_2 record. The calculated biospheric flux shows higher frequency variation after about 1800 compared with before. This is because the ice core record resolves more of the CO_2 variation after 1800, and the biospheric flux is calculated by tracking the spline fit to these measurements.

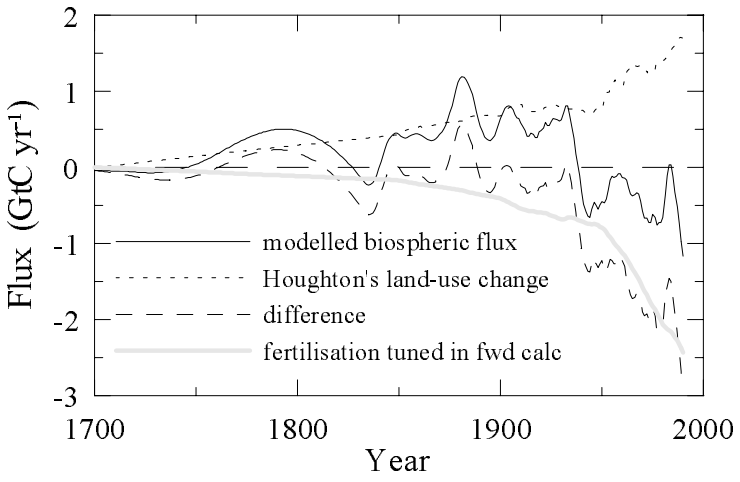

Figure 4.9: Biospheric flux from the single deconvolution calculation, the Houghton land-use change estimates and the deduced biospheric flux minus the land-use change estimates. The single deconvolution calculation includes the temperature increase over this century and temperature dependent ocean exchange, so the biospheric flux differs slightly from that in Figure 4.8. The thick grey line shows the net biospheric uptake due to CO_2 fertilisation from the forward model calculation.

The oceanic flux before 1800 appears to be anticorrelated with the biospheric flux but with a lag. This lagged anticorrelation is probably an artifact of the modelling, occurring because in the model the biospheric flux is calculated from the time derivative of the CO_2 concentration, while the oceanic flux responds to the CO_2 level. A double deconvolution, or a more complex ocean model, should give more realistic partitioning of CO_2 fluxes.

Figure 4.9 shows the biospheric flux and Houghton's estimates of the flux due to land-use change. The abrupt shift from a source to a sink in the deduced flux around the 1930s was also seen by Bruno and Joos (1997) and Craig et al. (1997). Figure 4.9 also shows the difference between the deduced flux and Houghton's land-use change estimates (dashed line). As found by Bruno and Joos (1997) and Craig et al. (1997), land-use change can explain the (long-term) variation in biospheric flux up to about 1930. After that time additional CO_2 uptake, perhaps CO_2 or nitrogen fertilisation, is required. The thick grey line in Figure 4.9 shows the uptake due to CO_2 fertilisation from the forward model calculation. The fraction of NPP fertilised by excess CO_2 was tuned to give the best fit to the observed CO_2 change, so the broad agreement of the magnitude of this flux with the 'difference' curve is not surprising. However, the temporal behaviour is

somewhat different. The difference curve is near zero until about 1930, then it drops rapidly. The fertilisation sink increases steadily up to 1950, then at a faster rate after 1950. As discussed in Section 2.11, Friedlingstein et al. (1995) calculated the fertilisation sink with a gridded biosphere model, and also found that the time evolution differed from that of the missing biospheric sink from a deconvolution. Their fertilisation sink was too high up to 1950 and too low between 1960 and 1980. They suggested that processes such as nitrogen deposition, climate variability or mid-latitude forest regrowth were required.

4.4.2 Bomb ^{14}C

Figures 4.8e - 4.8h show modelled ^{14}C during and after the bomb tests. There is generally good agreement with observations, although the tropospheric $\Delta^{14}C$ around 1965 is perhaps 100 ‰ too high, with modelled global levels looking almost like the northern hemisphere measurements. The bomb ^{14}C ocean inventory estimates are from Duffy and Caldeira (1995). The stratospheric data shown in Figure 4.8h are from Tans (1981), summarising measurements made by Telegadas (1971). The accuracy of these inventory estimates is questionable because the atmosphere would have been very inhomogeneous in the years soon after the bomb tests.

Hesshaimer et al. (1994) found a discrepancy in the budget of bomb ^{14}C when they compared model estimates of biospheric ^{14}C uptake and the change in ocean inventory of bomb ^{14}C (based on observations) with the observed change in the atmosphere. To balance the budget they required either 25 % less ocean uptake of ^{14}C than that suggested by GEOSECS data, or 80 % less biospheric uptake than that suggested by biosphere models. Joos (1994) compared the change in ^{14}C inventory from 1965 to 1989 for a number of models, and estimated a budget imbalance of $82 \pm 78 \times 10^{26}$ atoms when comparing the mean of the model estimates with observed atmospheric changes. Jain et al. (1997) claim that there is no discrepancy, given the large uncertainties involved, particularly in the stratospheric inventory, production rates of bomb ^{14}C and pre-bomb ocean $\Delta^{14}C$ values. Joos and Bruno (1998) suggested that estimates of the bomb test production and/or the stratospheric decrease are not compatible with ^{13}C and ^{14}C data.

The calculated changes in oceanic and biospheric ^{14}C inventory with the BDM from 1965–89 are 304 and 70 $\times 10^{26}$ atoms, respectively, and very close to the model averages given by Joos (1994). The model gives changes in tropospheric and stratospheric ^{14}C

from 1965–89 of 181 and 155 $\times 10^{26}$ atoms, respectively, both of which are higher than the observed changes quoted as 150 and 100 $\times 10^{26}$ atoms by Joos (1994). There does appear to be an imbalance in the budget, as suggested by Hesshaimer et al. (1994), however Figures 4.8e and 4.8h show that the fit to the available observations is reasonable, given the large uncertainties involved. If the model is calibrated without trying to match the stratospheric measurements, as was done by Lassey et al. (1996), then good agreement is found with all of the other measurements. The stratospheric turnover time chosen by the calibration procedure is quite fast. It seems likely that the calibration is giving turnover of the lower stratosphere rather than total stratosphere in order to match the stratospheric observations. This would mean that too much bomb ^{14}C is being put into the model, which may explain why the bomb ^{14}C production parameter is higher than its prior estimate. Clearly the bomb ^{14}C budget needs more work to understand it properly, but this is probably better done with a more complex model of the atmosphere than this simple 2-box model.

4.4.3 δ^{13}C

δ^{13}C is calculated as a 'by-product' in the single deconvolution calculation, and is due to the net fluxes that are determined from CO_2 and the ocean model, and the gross fluxes that are tuned for ^{14}C. Comparison of modelled and observed δ^{13}C is instructive, giving information on a number of aspects of the model calculation.

Industrial δ^{13}C decrease

The modelled δ^{13}C decrease over the industrial period agrees well with the Law Dome record, providing a valuable independent check on the calculation. Inclusion of the increase in temperature through the 20$^{\text{th}}$ century has a moderate effect on the modelled δ^{13}C (dashed curve in Figure 4.8b), but still permits reasonable agreement with the ice core measurements. Joos and Bruno (1998) also calculated the sensitivity to the change in isotopic fractionation of ocean exchange due to temperature and found that it made only a small difference to the calculated net fluxes in their double deconvolution, always less than 0.2 GtC y^{-1}. There are a number of other factors that could alter the match with the industrial δ^{13}C decrease that are not included in the BDM calculation. For example, a change in the ratio of C_3 to C_4 plants over time due to land-use change has probably

altered the globally averaged isotopic discrimination of the biosphere (Fung et al., 1997). If included in the model, this would give a slightly different change in δ^{13}C. Another is due to the fact that the CO_2 and δ^{13}C change measured in the Law Dome record applies for the high latitudes of the southern hemisphere, while the model considers global levels. The addition of fossil fuel CO_2 mainly in the northern hemisphere has caused the spatial distribution of CO_2 and δ^{13}C in the atmosphere to change over time, and therefore altered the difference between high southern latitudes and the global mean. In 1990, Law Dome CO_2 was about 2 ppm lower (R. M. Law, CRC-SHM, pers. comm), and δ^{13}C about 0.065 ‰ higher (Trolier et al., 1996), than the global average. Pre-industrially this difference was most likely considerably less than today, and possibly in the opposite direction (see Section 2.4). The single deconvolution calculation was run with an estimate of 'global' CO_2 constructed from the Law Dome measurements by adding an amount that increases (at a rate proportional to the CO_2 concentration) from zero in 1800 to 2 ppm in 1990. This calculation gives 0.04 GtC y^{-1} greater ocean uptake and 0.01 GtC y^{-1} less biospheric uptake in 1990 and leads to 0.03 ‰ greater decrease in the modelled δ^{13}C pre-industrial-to-modern change than using the Law Dome CO_2 record. Comparison of this 0.03 ‰ with the possible difference of 0.065 ‰ between the global and Law Dome δ^{13}C decreases suggests that the effect of ignoring the difference between Law Dome and global levels for δ^{13}C is partly compensated for by doing the same for CO_2. The difference $0.065 - 0.03 = 0.35$ ‰ is less than the uncertainty on the ice core measurements versus atmospheric levels of 0.05 ‰. This calculation does suggest that the δ^{13}C decrease was greater than is seen in the Law Dome measurements, which would give slightly worse agreement with the dashed line in Figure 4.8b.

Compared to the Law Dome ice core record, the South Pole firn record suggests a lower δ^{13}C level around 1900 (see Section 3.8), and therefore a smaller 1900-to-modern δ^{13}C decrease. Figure 4.10 shows the Law Dome CO_2 and δ^{13}C measurements and the single deconvolution results after 1850. Figure 4.10b also shows the South Pole firn δ^{13}C measurements prior to 1965 (after this time they agree with Law Dome). The modelled δ^{13}C with varying temperature (i.e. the dashed line) sits roughly between the Law Dome and the South Pole measurements. The earliest South Pole δ^{13}C measurement is quite a lot lower than the model values, although CO_2 is higher in this sample than expected when

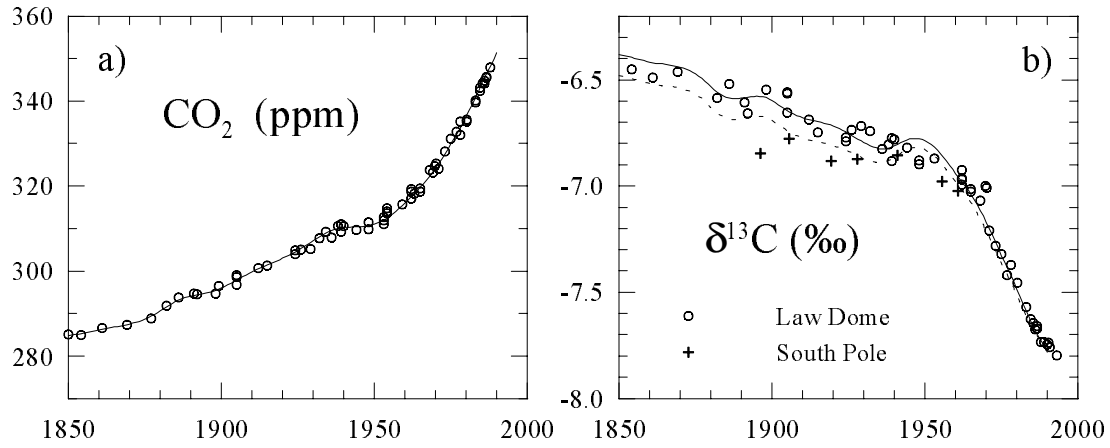

Figure 4.10: a) CO_2 and b) $\delta^{13}C$ from the single deconvolution model calculation and the Law Dome record. The dashed line in (b) is the single deconvolution result with varying temperature, as in Figure 4.8b. South Pole firn $\delta^{13}C$ measurements prior to 1965 are also shown.

compared with the Law Dome CO_2 record (Figure 3.30). The discrepancy between the Law Dome and South Pole $\delta^{13}C$ records needs to be resolved, which should be possible with more measurements that take care to avoid the problems mentioned in Section 3.8. The $\delta^{13}C$ decrease should then be quite a strong constraint, particularly if the uncertainties on the ice core measurements relative to atmospheric levels are around (or less than) the value of 0.05 ‰ given by Francey et al. (1999a). The $\delta^{13}C$ change calculated by a carbon cycle model depends on a number of factors affecting how both the net and gross fluxes influence $\delta^{13}C$. The net and gross fluxes are both known to some degree from other methods (the gross fluxes from ^{14}C and the net fluxes from methods such as ocean models or oxygen budgets). The usual aim for $\delta^{13}C$ is to help determine the net fluxes, which is only possible if the effect of the gross fluxes on ^{13}C is well enough known.

The $\delta^{13}C$ budget in terms of the isotopic anomaly, X, was described in Section 2.5. Figure 4.11 (similar to a figure by Joos and Bruno, 1998) shows the variation of terms in the anomaly budget with time from the single deconvolution calculation. The isoflux terms (gross bio $= F_{ba}(\delta_a^b - \delta_a)$; gross ocn $= F_{oa}(\delta_a^o - \delta_a)$) are larger than the net flux terms near the end of the calculation. If the isoflux uncertainties are also large, then ^{13}C may not be so useful for estimating net fluxes. The isofluxes and their uncertainties will be discussed in Section 6.1.

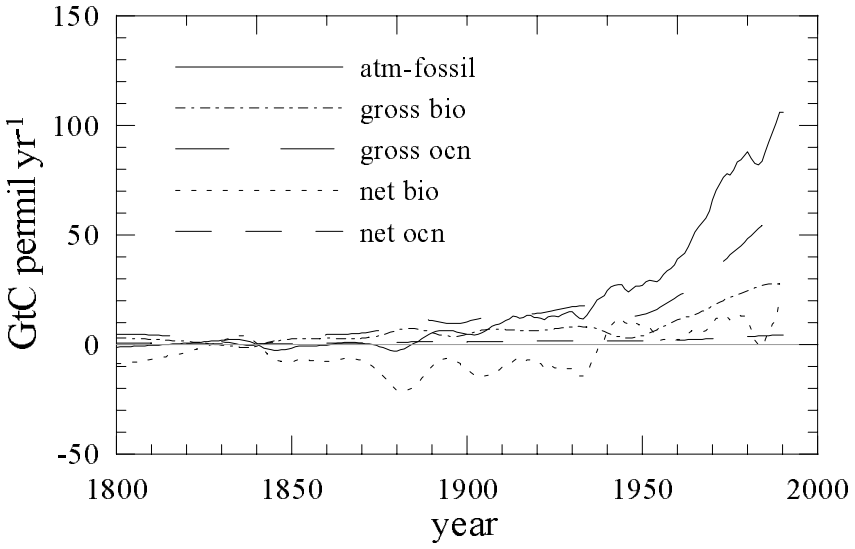

Figure 4.11: Budget of the isotopic anomaly, X, as fluxes in GtC ‰ y^{-1} for the single deconvolution BDM run.

Variability in $\delta^{13}C$

The CO_2 spline in Figure 4.10 shows a number of decadal time scale features. Tracking the CO_2 curve with the single deconvolution has produced similar features in the modelled δ^{13}C. The δ^{13}C features are more pronounced than the corresponding CO_2, as described in Section 4.3.3. This decadal δ^{13}C variation can be compared with the Law Dome measurements. The strongest feature in the model output is the peak in δ^{13}C in the 1940s and 1950s, which doesn't appear to be seen in the measurements. The suggestion from this is that the CO_2 flattening around this time may be due to oceanic rather than biospheric fluxes (in the single deconvolution the model assumed that it was biospheric). Francey et al. (1999a) described the 'step-like' behaviour of the Law Dome δ^{13}C through the industrial period. Figure 4.12 (the same as Figure 11 in Francey et al., 1999a) shows δ^{13}C plotted as a function of CO_2. The solid line shows the spline fits to the ice core CO_2 and δ^{13}C measurements (created as a function of time), while the dashed line shows the single deconvolution results. Both curves use the same CO_2 spline. Francey et al. (1999a) noted that the solid line is more step-like than the dashed line, and that the multi-decadal variability in δ^{13}C is greater than would be expected just due to the fact that the response functions for δ^{13}C and CO_2 are different. It is possible that this may be due to variability

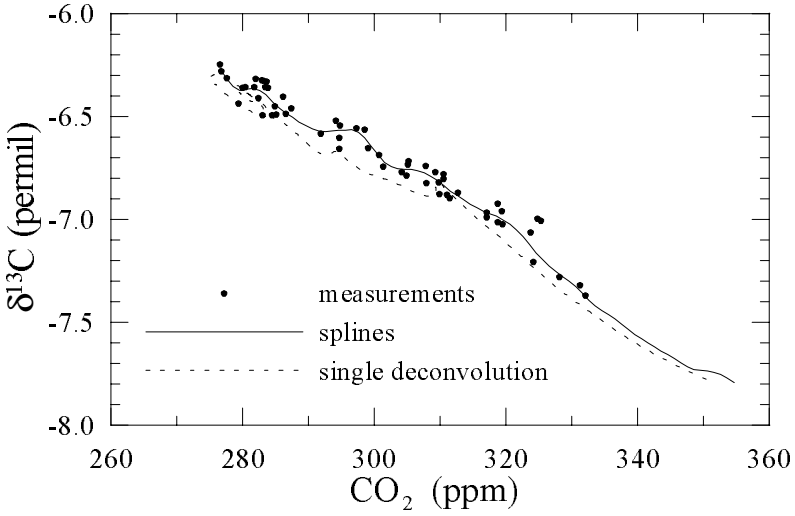

Figure 4.12: δ^{13}C versus CO_2. The solid line shows spline fits to the CO_2 and δ^{13}C measurements and the dashed line shows output from the single deconvolution model calculation.

in the isofluxes, or due to scatter in the δ^{13}C measurements. It could also be due to the fact that there is more 'information' about the net fluxes in the δ^{13}C measurements. Further discussion will be given in Chapter 6.

Mixed layer $\delta^{13}C$

Figure 4.13 shows the δ^{13}C in the mixed layer from the single deconvolution calculation with three of the δ^{13}C sponge records of Böhm et al. (2000). The sponge records are from different depths in the ocean. The overall decrease in δ^{13}C in the model is not expected to agree with the decrease measured in the sponge records, since these are for a particular depth, while the model gives the change for a well mixed 75 m layer. Local circulation will also affect the sponge records (Böhm et al., 1996). However, features in the records can be compared with the model output. The Ce96 sponge record shows high levels of δ^{13}C between about 1650 and 1750. The timing of the δ^{13}C increase in the single deconvolution roughly agrees with the Ce96 record. The deeper Pedro Bank sponge record shows much less δ^{13}C increase in the LIA.

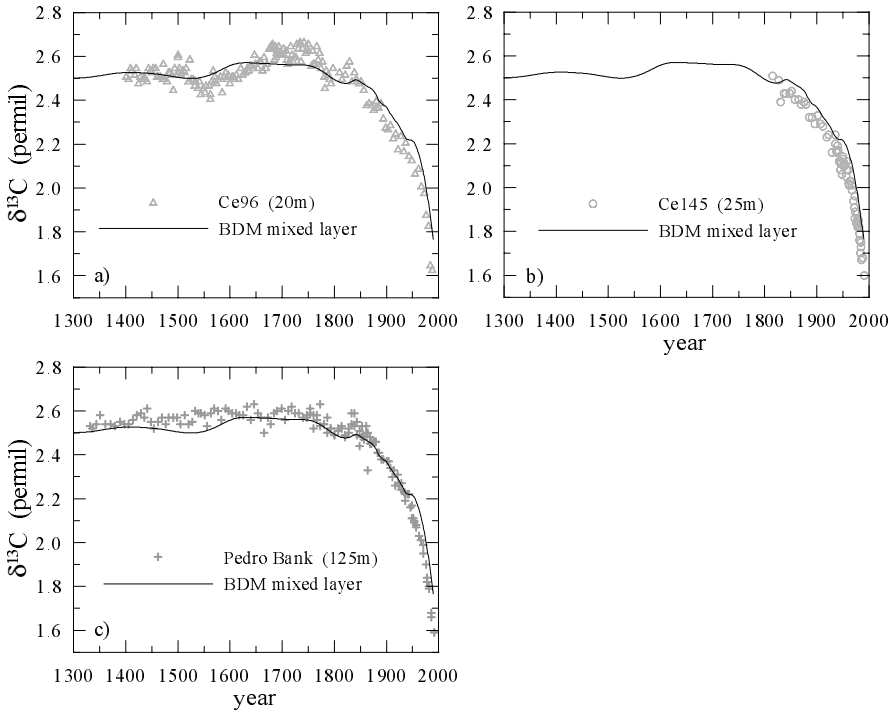

Figure 4.13: Mixed layer δ^{13}C from the single deconvolution calculation and the sponge records from Böhm et al. (2000) measured at a) Montego Bay (Ce96) b) Rio Bueno (Ce145) and c) Pedro Bank (392-19).

4.5 Concluding remarks

This chapter contains description of a number of forward and single deconvolution calculations with the box diffusion carbon cycle model. The single deconvolution calculation has been performed before with the Law Dome CO_2 record (Bruno and Joos, 1997; Craig et al., 1997), but here the results are compared with the Law Dome δ^{13}C record.

There is general agreement of the forward calculation with Law Dome CO_2 and δ^{13}C. The δ^{13}C decrease over the industrial period, which depends on the gross fluxes tuned to ^{14}C, is very good. There are a number of multidecadal to century time scale variations in the CO_2 and δ^{13}C observations that are not predicted by the model with the inputs that are used. A major feature is the decrease in CO_2, and corresponding increase in δ^{13}C, through the LIA period. Model calculations suggest that the observed changes are due to the response of the land, rather than oceans, to lower temperatures. ^{14}C is very important in model calibration, although improving the fit to pre-bomb Δ^{14}C by including

time variations in the natural production rate from a ^{10}Be record does not help constrain the model parameters. This suggests that the bomb pulse is giving the most information for model calibration.

The single deconvolution calculation also showed good agreement with the overall decrease in atmospheric δ^{13}C. The temperature decrease over this century reduces the δ^{13}C change by about 0.1 ‰. δ^{13}C from the model (with the temperature decrease) sits mid-way between the Law Dome record and the South Pole firn record in the first half of the 20$^{\text{th}}$ century. There are a number of factors not included in the model that could alter this change. These are generally below the uncertainty in the δ^{13}C data. The variability of δ^{13}C predicted by the model in the atmosphere was briefly compared with observations. More discussion of this comparison will be given in Chapter 6. The model calculations presented in this chapter would support recent findings that the budget of bomb ^{14}C is not exactly balanced.

Temperature records generally reflect local as well as global variations. Ice core records of long-lived trace gases from Antarctica, however, record smoothed, global signals because the diffusion and trapping processes involved in storing air in the ice lead to a smoothing of at least 10 years (see Chapter 3), the trace gases are generally well mixed in the atmosphere and Antarctica is remote from terrestrial sources and sinks. These calculations have illustrated how ice core records of long-lived trace gases have the potential not only to provide information on the carbon cycle, but also on aspects of the climate of the past.